Ocean bottom profiling with ambient noise: A model for the passive fathometer

James Traer, [a] Peter Gerstoft, and William S. Hodgkiss
Marine Physical Laboratory, Scripps Institution of Oceanography, La Jolla, California 92093-0238

(Received 28 April 2010; revised 3 January 2011; accepted 5 January 2011)

A model is presented for the complete passive fathometer response to ocean surface noise, interfering discrete noise sources, and locally uncorrelated noise in an ideal waveguide. The leading order term of the ocean surface noise contribution produces the cross-correlation of vertical multipaths and yields the depth of sub-bottom reflectors. Discrete noise incident on the array via multipaths give multiple peaks in the fathometer response. These peaks may obscure the sub-bottom reflections but can be attenuated with use of minimum variance distortionless response (MVDR) steering vectors. The seabed critical angle introduces discontinuities in the spatial distribution of distant surface noise and may introduce spurious peaks in the passive fathometer response. These peaks can be attenuated by beamforming within a bandwidth limited by the array geometry and critical angle.
 [DOI: 10.1121/1.3552871]

PACS number(s): 43.30.Wi, 43.30.Pc, 43.60.Pt, 43.30.Nb [AIT] Pages: 1825–1836

I. INTRODUCTION

Ambient noise, which has long been considered an experimental nuisance, contains information from which environmental parameters can be inferred[1,2] and correlations of oceanic ambient noise allows inference of medium properties.[3–6] Application of array processing techniques enhance the fidelity of such correlations and may improve the performance of geophysical inversions of ambient noise.

One such array processing technique, beamforming on a vertical hydrophone array, can focus on vertically propagating noise that contains noise reflected from and therefore information about the seabed. This can be used to infer ocean bottom properties such as seabed critical angle,[7,8] reflection loss versus angle of incidence[9] and the depth of sub-bottom reflection layers.[10–16] The process of obtaining the latter by cross-correlating noise is referred to as passive fathometry. The noise source for the passive fathometer is wind and wave generated surface noise, which is often modeled as an infinite sheet of surface noise sources.[17–19] These models imply that there is much more acoustic energy propagating horizontally in the waveguide than vertically, and, hence, directional sensitivity attained by adaptive beamforming[15] and/or velocity sensors[11] may yield an improvement in the passive fathometer response.

Recent experiments with a drifting vertical array[20] have shown that the bottom reflection can be obscured by interference from shipping noise.[15] In order to determine the practical limits of the passive fathometer, a detailed analysis of its response to arbitrary noise fields is required. We use a simple ocean noise model[21] with three sources: correlated noise generated near the ocean surface by the action of wind and waves, discrete noise generated by point sources at arbitrary positions in the water column (i.e., ships), and spatially uncorrelated white noise due to electrical noise within the array. Both conventional and adaptive beamforming are considered.

As beamforming increases the contribution of vertically propagating noise to the passive fathometer response, a simple model is first considered in which the ocean surface produces only vertically propagating plane waves. This model allows many of the features of the passive fathometer response to be addressed qualitatively with a minimum of algebra. The passive fathometer model presented here also considers spatial aliasing, in which the array gain is applied to noise toward which the array is not intentionally steered.

Depending on the dimensionality of the system and noise source, the time domain Green's function can be proportional to the noise cross-correlation, its time derivative, time integral, or fractional derivative.[11,22] Assuming that the dominant component of the passive fathometer response is due to vertically propagating noise, the system is approximately one-dimensional (1D) and thus the Green's function is proportional to the noise correlation.

Prior models for the passive fathometer response have either numerically evaluated the integration over the ocean surface,[10–12] or assumed that the array is preferentially sensitive to vertically propagating noise in order to make the surface integration tractable.[11,12] The model presented here details how beamforming attenuates horizontally propagating signals (Sec. II) and how the stationary phase approximation shows that the cross-correlation of vertically separated sensors under an infinite surface sheet of noise is preferentially weighted toward vertically propagating noise (Appendix A). Thus the leading order behavior is computed analytically.

The model presented is restricted to a horizontally stratified waveguide with a constant sound speed profile in the water column and a perfectly uncorrelated surface sheet of noise sources. These approximations are not sufficient to describe a real ocean; however small variations from this model will not affect the leading order characteristics of the model passive fathometer response.

[a]Author to whom correspondence should be addressed. Electronic mail: jtraer@ucsd.edu

II. THEORY

Consider an m-element vertical array positioned in a water column of depth Δ and uniform sound speed c (Fig. 1). Define the bottom hydrophone depth as z_a and the inter-element separation as d, such that the inter-element travel time is $\tau = d/c$. It is convenient to define $\psi = e^{i\omega\tau}$, where ω is the angular frequency. In the frequency domain, multiplication of the data from the pth hydrophone, $x_p(\omega)$, by ψ is equivalent to shifting in the time domain by τ to yield $x_p(t+\tau)$. The array beam steered to add in phase vertically downward propagating noise D, and the corresponding beam steered to add in phase vertically upward propagating noise U, are

$$D(\omega) = \sum_{p=1}^{m} \psi^{-(p-1)} x_p(\omega) = \mathbf{w}^H \mathbf{x}$$
$$U(\omega) = \sum_{p=1}^{m} \psi^{(p-1)} x_p(\omega) = \mathbf{w}^H \mathbf{x}, \quad (1)$$

where we have defined the steering vector for downward propagating noise as

$$\mathbf{w}^T = [1, \psi, \psi^2, \ldots, \psi^{(m-2)}, \psi^{(m-1)}], \quad (2)$$

and the reference phone ($p=1$) is the lowermost element. The superscripts T and H represent a matrix transpose and Hermitian transpose, respectively, such that $\mathbf{w}^H = (\mathbf{w}^*)^T$.

Consider a simple ocean noise model in which the environment is range independent and surface noise is spatially uncorrelated. Define the sound incident on the above array as

$$\mathbf{x}(\omega) = \int_{r=0}^{\infty} \mathbf{g}(r, z = z_0; z_p) s(r, \omega) 2\pi r dr + \sum_{j=1}^{J} \mathbf{g}(r_j, z_j; z_p) n_j(w) + \mathbf{u}, \quad (3)$$

where $s(r,\omega)2\pi r\, dr$ is the signal generated by the annulus of ocean surface around the array between radii r and $r+dr$,

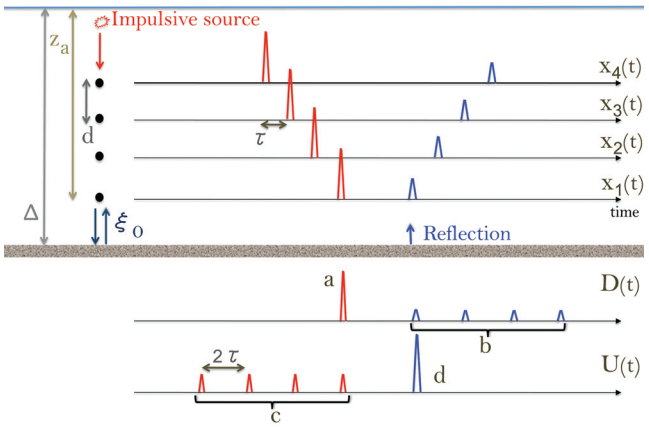

FIG. 1. (Color online) Key variables in the analytical description of the passive fathometer. The water column depth, Δ, the depth of the lowermost array element, z_a, the inter-element separation, d, the inter-element propagation time for vertical signals, τ, the two-way travel distance between the array and seabed, ξ_0, the data from the pth hydrophone, $x_p(t)$. $D(t)$ and $U(t)$ are the time domain form of the beams defined in Eq. (1). a, b, c, and d are the key features within these beams.

$\mathbf{g}(r, z; r_p, z_p)$ is a vector of Green's functions from the source at depth z and radial distance r to each hydrophone at depth z_p. z_0 is a depth near the ocean surface. The integral over r accounts for the noise generated by the ocean surface, which is assumed infinite. Assuming the presence of J discrete sources with frequency-dependent amplitude $n_j(\omega)$, $\mathbf{g}(r_j, z_j)$ is a vector of Green's functions from each discrete source to the array. $\mathbf{u}$ denotes the uncorrelated white noise at each element. These three terms are referred to as the correlated noise, discrete noise, and white noise.[21] These terms are assumed to be independent.

Using the steering vector as defined in Eq. (2), the fathometer response is[11]

$$C(\omega) = \mathbf{w}^T \mathbf{R}(\omega) \mathbf{w}, \quad (4)$$

with cross-spectral density matrix (CSDM), $\mathbf{R}$ given by

$$\mathbf{R}(\omega) = E[\mathbf{x}(\omega)\mathbf{x}^H(\omega)], \quad (5)$$

where $E[]$ denotes the expectation operator. As detailed in Appendix A, substituting Eqs. (3) and (5) into Eq. (4) gives the fathometer model response as

$$C(\omega) = |S(\omega)|^2 \int_{r=0}^{\infty} \mathbf{w}^T \mathbf{g}\mathbf{g}^H \mathbf{w} 2\pi r dr + \sum_{j=1}^{J} |N_j(\omega)|^2 \mathbf{w}^T \mathbf{g}_j \mathbf{g}_j^H \mathbf{w} + \sigma^2 \mathbf{w}^T \mathbf{I} \mathbf{w} \quad (6)$$

where $\mathbf{I}$ denotes the identity matrix, $|S(\omega)|^2$ is the power spectrum per unit area of the surface noise with absolute magnitude independent of r and $|N_j(\omega)|^2$ is the power spectrum of the jth source. The individual terms are now examined in detail. A final subsection (Sec. II D) will consider the effect of minimum variance distortionless response (MVDR) beamforming.

A. White noise

The white noise component of the fathometer response is given by

$$\sigma^2 \mathbf{w}^T \mathbf{I} \mathbf{w} = \sigma^2 \sum_{p=1}^{m} \psi^{(p-1)} \psi^{(p-1)} = \sigma^2 \Psi, \quad (7)$$

where $\Psi = \sum_p \psi^{2(p-1)}$. Assuming infinite bandwidth, each term in the summation gives a δ-function in the time domain located at $-2(p-1)\tau$. With a finite bandwidth the δ-functions become peaks of finite width with heights that scale with σ^2. The summation results in m equispaced δ-functions between $t = -2(m-1)\tau$ and $t = 0$. This is the only region in the time domain fathometer response that shows contribution from uncorrelated noise. As this region will be referred to repeatedly in this analysis, it is designated the sensor noise region.

B. Correlated noise

The correlated noise component contains an integral over the infinite ocean surface [Eq. (6)]. Before considering

this integral in detail (Sec. II B 2 and Appendix A) the leading order behavior can be obtained by considering the array response to a 1D vertical noise field. Neglecting non-vertical noise can be justified for two reasons: (1) contributions to the cross-correlation from sources situated on a ray-path that passes directly through both sensors are added in phase and hence are preferentially weighted[23,24] and (2) the preferential weighting of vertical noise is increased by beamforming [Eq. (1)] and more so by MVDR beamforming. In Sec. II B 2 this will be shown to be a good first order approximation.

1. Vertical noise model

Assuming the surface signal is generated by a point source at $r=0$ and depth z_0, $s(r,\ z,\ \omega)=\delta(r)\delta(z-z_0)s(\omega)$. Substituting the correlated term from Eq. (3) into Eq. (5) gives the component of the CSDM due to correlated noise,

$$\mathbf{R}_c(\omega)=|S(\omega)|^2\mathbf{g}(r=0,z=z_0;z_p)\mathbf{g}(r=0,z=z_0;z_p)^H. \tag{8}$$

The Green's function for the pth hydrophone is

$$[\mathbf{g}]_p=e^{-\imath\omega(z_a-z_0)/c}\left[\psi^{(p-1)}+\psi^{-(p-1)}\sum_l^L\Gamma_l e^{-\imath\omega\xi_l/c}\right], \tag{9}$$

where the first term accounts for the downward propagating path and the summation accounts for a set of upward propagating reflections. Γ_l is the reflection coefficient of the lth reflecting layer and ξ_l is twice the distance from the array bottom, z_a to the lth layer. We assume no reflections between layers or reflections from the ocean surface as, assuming the reflection coefficient from each interface is small, the contribution from paths involving multiple reflections are negligible. Expanding the following analysis to include arbitrary reflections is conceptually simple and algebraically tedious and is described in Appendix A 2.

Using the steering vector defined in Eq. (2), the vector of Green's functions for the array can be written as

$$\mathbf{g}=e^{-\imath\omega(z_a-z_0)/c}[\mathbf{w}+H(\omega)\mathbf{w}^*], \tag{10}$$

where $H(\omega)$ is seabed transfer function,

$$H(\omega)=\sum_l^L\Gamma_l e^{-\imath\omega\xi_l/c}, \tag{11}$$

and Γ_l is the reflection coefficient of the lth interface.

Substituting Eqs. (10) and (11) into Eq. (8) gives the CSDM elements,

$$[\mathbf{R}_c]_{pq}=|S(\omega)|^2[(1+|H|^2)\psi^{q-p}+H\psi^{-(p+q-2)}+H^*\psi^{(p+q-2)}], \tag{12}$$

which, using Eq. (4), gives the passive fathometer response component due to correlated noise,

$$C_c(\omega)=|S(\omega)|^2[m^2H+(1+|H|^2)m\Psi+H^*\Psi^2]. \tag{13}$$

Transforming to the time domain gives

$$C_c(t)=\zeta(t)*(T_1+T_2+T_3+T_4), \tag{14}$$

where * denotes convolution and

$$\begin{aligned}T_1&=m^2\sum_l\Gamma_l\delta(t-\xi_l/c)\\ T_2&=m\sum_{p=1}^m\delta(t+2(p-1)\tau),\\ T_3&=\eta(t)*T_2(t)\\ T_4&=m\sum_{l=1}^L\sum_{p=1}^{2m}\left(1-\left|1-\frac{p}{m}\right|\right)\\ &\quad\times\Gamma_l\delta(t+\xi_l/c+2(p-1)\tau),\end{aligned} \tag{15}$$

where $\zeta(t)$ is the inverse Fourier transform of $|S(\omega)|^2$ (and therefore the autocorrelation of the surface noise). As the surface noise is assumed to be white and band limited, $\zeta(t)$ is a sinc-function with the pulse-width determined by the processing bandwidth. $\delta(t)$ is the Dirac δ-function and $\eta(t)$ is the time domain representation of $|H(\omega)|^2=(\Sigma_j\Gamma_j e^{-\imath\omega\xi_j/c})(\Sigma_l\Gamma_l e^{\imath\omega\xi_l/c})$,

$$\eta(t)=\sum_{j,l}^L\Gamma_j\Gamma_l\delta\left(t-\frac{\xi_j-\xi_l}{c}\right). \tag{16}$$

The schematic form of these terms is shown in Fig. 2.

All of the terms T_1-T_4 in the time domain are formed by the summation of m^2 δ-functions, each corresponding to one element of the $m\times m$ CSDM [Eq. (12)]. Due to the action of the steering vectors all the δ-functions in T_1 are produced at the same position for all values of p and q [Eq. (13)], resulting in a single peak with amplitude increased by a factor of m^2 for each reflecting layer. T_1 and T_4 are the contribution of the up-going and down-going signals correlated with each

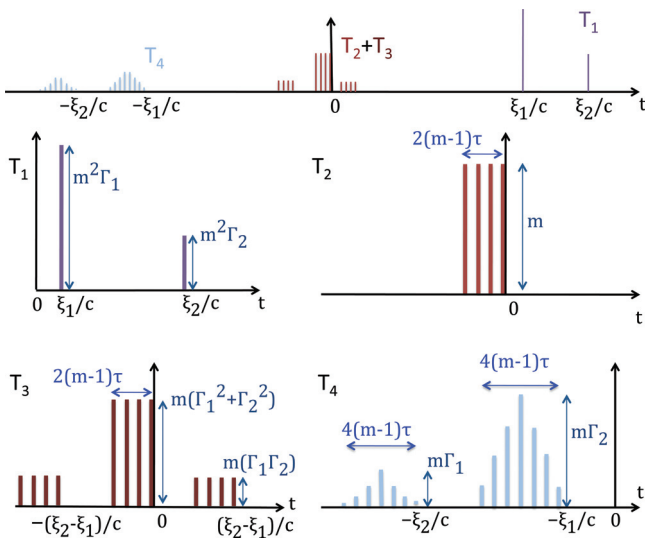

FIG. 2. (Color online) Schematic of the terms from Eq. (15) for the case of a four element array ($m=4$) and two reflecting layers. The horizontal axis is time and the vertical axis is the passive fathometer response. The top plot is the complete time series with the lower four examining the individual components. Note the array gain of m^2 applied to T_1.

other and the m^2 gain applied to T_1 is consistent with both the vertical up-going and down-going signals subject to an array gain of m, Ref. 25. This is the feature of interest for ocean bottom profiling and, other than T_3, which is scaled by Γ^2 and is likely to be small amplitude, T_1 is the only term due to surface noise that contains peaks at positive correlation times.

T_4 gives L sets of $2m$ δ-functions [the position of the m^2 δ-functions is now a function of p and q, Eq. (13)] between $t = -\xi_l/c - 4(m-1)r$ and $t = -\xi_l/c$, the latter of which is the negative of the two-way travel time of the lth layer. T_2 [produced by the autocorrelation of the down-going signal, Eq. (10)] gives a set of m equispaced δ-functions in the sensor noise region of amplitude m, as the δ-function location is now a function of p only. T_3 (up-going signal) gives the same δ-functions convolved with the seabed impulse response and its time-reversed form.

2. Inclusion of non-vertical noise

The analysis of Sec. II B 1 is now expanded to include signal contributions from an infinite ocean surface. The Green's function between a source at $\mathbf{r} = (r, z)$ and a receiver at $\mathbf{r}_p = (0, z_p)$ in a waveguide is[24–26]

$$G(\mathbf{r}_p;\mathbf{r}) = \sum_{\alpha}^{1} \Gamma^{b_\alpha} \frac{e^{\imath(\omega/c)L_\alpha(\mathbf{r}_p,\mathbf{r})}}{4\pi L_\alpha(\mathbf{r}_p,\mathbf{r})}, \tag{17}$$

where the subscript α distinguishes between different multipaths and b_α is the number of reflections from the seabed in the α path. L_α the travel distance from receiver to source along the α path. Substituting Eq. (17) into the correlated component of Eq. (6), the integral over r can be computed by the stationary phase approximation[23,24,27] and, as detailed in Appendix A, assuming one seabed reflecting layer, a reflection coefficient Γ independent of grazing angle and no surface reflections, this result can be simplified to yield

$$C_c(\omega) = \frac{-\imath c|S(\omega)|^2}{8\pi\omega} \sum_{p=1}^{m}\sum_{q=1}^{m} \left[(1+\Gamma^2)\frac{\psi^{2(q-1)}}{(q-p)d} + \Gamma \frac{\psi^{-\xi_0/d} + \psi^{\xi_0/d+2(p+q-2)}}{\xi_0 + (p+q-2)d} \right] \forall p \neq q. \tag{18}$$

This is a summation of terms of the general form $B(p, q)\psi^{\mu(p,q)}$ which gives a set of δ-functions of amplitude $B(p, q)$ at location $-\mu(p,q)\tau$ in the time domain. Thus the first term in the response in Eq. (18), in the time domain, is a set of δ-functions at $-\mu\tau = -2(q-1)\tau$ with an amplitude of $B = c|S|^2(1+\Gamma^2)/[(q-p)d]$ for all values of $p \neq q$. The fathometer response has a $1/\omega$ dependence, consistent with other analytical treatments of ambient noise cross-correlations in three dimensions (3D).[22,24] This can be removed by the multiplication by ω, which is equivalent to a differentiation with respect to time in the time domain.

The terms in Eq. (18) are produced in the same locations as those in Eq. (15) and differ only in amplitude. The $\psi^{2(q-1)}$ term corresponds to $T_2 + T_3$, assuming only a single reflection from the seabed. The $\psi^{-\xi_0/d}$ term corresponds to T_1 and produces a single peak at ω_0/c. The $\psi^{\xi_0/d+2(p+q-2)}$ term corresponds to T_4.

Note that the diagonal terms ($p = q$) of Eq. (18) are infinite. This is because the diagonal terms consist of autocorrelations for which the phase variation between the signals is zero and the stationary phase approximation is not valid.

C. Discrete sources

For simplicity, we consider a single discrete source ($J = 1$) in the waveguide described in Sec. II B 2. The analysis is extended to include more layers and higher-order reflections in Appendix A and moving sources in Appendix B. In this case there are six distinct paths that undergo a single seabed reflection as shown in Fig. 3. In Fig. 3 the propagation paths are straight lines as the sound speed is constant throughout the water column. Introducing a variable sound speed will lead to curved paths that are algebraically more complex to describe. However it is still the path length difference between multipaths that determines the position of the correlation peak. Substituting Eq. (17) into the discrete component of Eq. (6) and allowing for six possible multipaths [Fig. 3(a)] gives the component of the passive fathometer response due to discrete noise,

$$C_d(\omega) = \sum_{p,q=1}^{m}\sum_{\alpha,\beta=0}^{6} |N_j(\omega)|^2 \frac{\Gamma^{b_\alpha+b_\beta}}{(4\pi)^2 L_\alpha L_\beta} \psi^{(p+q-2)+(L_\alpha-L_\beta/d)} = \sum_{p,q=1}^{m}\sum_{\alpha,\beta=0}^{6} B(p,q,\alpha,\beta)\psi^{\mu(p,q,\alpha,\beta)} \tag{19}$$

where p and q denote the indices of the array elements.

Assuming infinite bandwidth, each term $B\psi^\mu$ gives a δ-function in the time domain at $-\mu\tau$ with an amplitude B. Assuming paths α and β are incident on the array as plane waves incident at angles ϕ_α and ϕ_β to the horizontal the path length differences of the α and β rays incident on the pth and qth elements, respectively, can be computed geometrically, as shown in Fig. 3(b). This yields

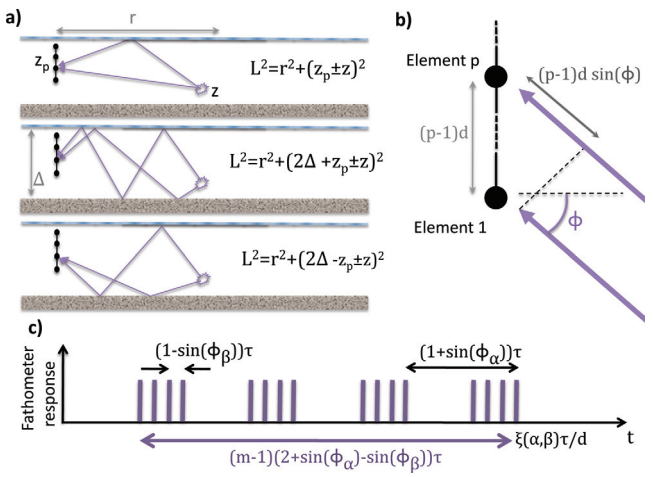

FIG. 3. (Color online) (a) Multipaths in a waveguide with no more than one seabed reflection. (b) The phase difference between the lowermost element and the pth element is given by $(p-1)d \sin \phi$ where ϕ is the angle of incidence. (c) Time domain fathometer response induced by the correlation of two δ-functions incident from angles ϕ_α and ϕ_β on a four element array.

$$\mu = (p+q-2) - \frac{L_\beta - L_\alpha}{d}$$
$$= (p-1)(1+\sin\phi_\alpha) + (q-1)(1-\sin\phi_\beta) - \frac{\xi(\beta,\alpha)}{d}, \quad (20)$$

where $\xi(\beta,\alpha)$ is the path length difference at the lowermost hydrophone of the array. As such, signals with correlated multipaths will give sets of m^2 δ-functions at times $\xi/c - 4(m-1)\tau \le t \le \xi/c$. The δ-functions will be spread over the entirety of this region if $\sin\phi_\alpha = 1$ and $\sin\phi_\beta = -1$, which occurs when both signals are vertical and is directly analogous to T_4 (Sec. II B 1). For any other values of ϕ_α and ϕ_β the δ-functions will be spread over a smaller region, as illustrated in Fig. 3(c). When a source is close enough to the array that the plane wave approximation is not valid, the peak locations will be slightly perturbed from the values presented here.

If $\alpha = \beta$ (equivalent to autocorrelating a signal as it implies identical travel paths), then $\xi(\alpha, \alpha) = 0$ and μ is constrained to be $0 < \mu < 2(m-1)\tau$. When summed over p and q, this gives a set of δ-functions in the sensor noise region.

Every pairwise combination of $\alpha \neq \beta$ produces two sets of m^2 δ-functions (one set at positive and one set at negative correlation time offsets, between $\pm\xi/c - 4(m-1)\tau$ and $\pm\xi/c$). A discrete source incident on the array via N significant multipaths will therefore produce $N(N-1)/2$ sets in the positive time domain that may obscure the seabed response.

D. MVDR fathometer processing

MVDR processing has been used to improve the passive fathometer response in the presence of interfering noise.[11–15] It is identical to the processing described in Sec. II A–C with the steering vectors in Eq. (4) replaced by the MVDR steering vectors for upward and downward propagating waves,[28]

$$\tilde{\mathbf{w}}_U = \frac{\mathbf{R}^{-1}\mathbf{w}^*}{\mathbf{w}^T\mathbf{R}^{-1}\mathbf{w}^*}$$
$$\tilde{\mathbf{w}}_D = \frac{\mathbf{R}^{-1}\mathbf{w}}{\mathbf{w}^H\mathbf{R}^{-1}\mathbf{w}}, \quad (21)$$

where $\tilde{}$ indicates use of MVDR processing. Substituting these steering vectors into Eq. (4) gives the MVDR passive fathometer response,

$$\tilde{C}(\omega) = \tilde{\mathbf{w}}_U \mathbf{R} \tilde{\mathbf{w}}_D = \Lambda \mathbf{w}^T \mathbf{R}^{-1} \mathbf{w}, \quad (22)$$

where $\Lambda = |\mathbf{w}^H\mathbf{R}^{-1}\mathbf{w}|^{-2}$ is a positive normalization factor. Other adaptive processing methods with additional constraints may be used and as also they provide a greater weighting to vertically propagating contributions they will yield a similar response. Given $J+1$ sources incident on the array [from J discrete interferers and the vertical component of the correlated noise, which is designated as the $(J+1)$th correlated signal and is asymptotically dominated by vertically propagating noise (Appendix A) and hence can be accounted for with a single eigenvector], an eigendecomposition of the CSDM gives

$$\mathbf{R} = \sum_{j=1}^{J+1} (b_j + \sigma^2)\mathbf{u}_j\mathbf{u}_j^H + \sum_{j=J+2}^{m} \sigma^2 \mathbf{u}_j\mathbf{u}_j^H, \quad (23)$$

where b_j is the component of the eigenvalue due to the jth coherent source and scales as the trace of the CSDM associated with the jth coherent signal (i.e., $|N_j|^2\mathbf{g}_j\mathbf{g}_j^{\mathrm{H}}$ for all $j \le J$ and $|S(\omega)|^2 \int \mathbf{g}\mathbf{g}^H\, 2\pi r\, dr$ for $j = J+1$). The matrix inverse is then[14]

$$\mathbf{R}^{-1} = \sum_{j=1}^{J+1} \frac{1}{(b_j+\sigma^2)}\mathbf{u}_j\mathbf{u}_j^H + \sum_{j=J+2}^{m} \frac{1}{\sigma^2}\mathbf{u}_j\mathbf{u}_j^H$$
$$= \frac{1}{\sigma^2}\left[\sum_{j=1}^{J+1} \frac{\sigma^2}{(b_j+\sigma^2)}\mathbf{u}_j\mathbf{u}_j^H + \mathbf{I} - \sum_{j=1}^{J+1}\mathbf{u}_j\mathbf{u}_j^H\right]$$
$$= \frac{1}{\sigma^2}\left[\mathbf{I} - \sum_{j=1}^{J+1}\frac{b_j\mathbf{u}_j\mathbf{u}_j^H}{(b_j+\sigma^2)}\right] = -\frac{|S(\omega)|^2\mathbf{g}\mathbf{g}^H 2\pi r\, dr}{(b_{J+1}+\sigma^2)^2}$$
$$- \sum_{j=1}^{J}\frac{|N_j(\omega)|^2\mathbf{g}_j\mathbf{g}_j^H}{(b_j+\sigma^2)^2} + \frac{1}{\sigma^2}\mathbf{I}, \quad (24)$$

where we have utilized $\sum \mathbf{u}_j\mathbf{u}_j^H = \mathbf{I}$.This contains the same components as the CSDM [Eq. (A1) in Appendix A] due to correlated noise, J discrete interferers and white noise, but all except the component due to incoherent noise have been multiplied by negative factors. This is consistent with previous models that considered only surface noise[13] and surface noise as well as sensor noise.[14]

Note that each component of the matrix inverse is scaled by $1/(b_j+\sigma^2)$. This acts to attenuate the contribution of strong signals to the fathometer response. The normalization factor is equivalent to[28]

$$\Lambda(\omega) = U_{\mathrm{MVDR}}(\omega) D_{\mathrm{MVDR}}(\omega), \quad (25)$$

where $U_{\mathrm{MVDR}} = (\mathbf{w}^T\mathbf{R}^{-1}\mathbf{w}^*)^{-1}$ and $D_{\mathrm{MVDR}} = (\mathbf{w}^H\mathbf{R}^{-1}\mathbf{w})^{-1}$ are the estimates of the up- and downward propagating spectral power obtained by the MVDR beamformer. This term is large at frequencies with large power contributions from vertical directions and will counteract the attenuation due to the $1/(b_{J+1}+\sigma^2)$ factor.

Thus the MVDR fathometer response is qualitatively similar to that of the conventional passive fathometer but all components except that due to incoherent noise are multiplied by a negative factor[13,14] and the contribution from nonvertical sources is reduced by a factor proportionate to the power of that signal incident on the array.

III. NUMERICAL SIMULATION

A. Two-dimensional noise model

A simple fathometer model was generated assuming only vertically propagating surface noise, one discrete source, and sensor noise. The discrete source is assumed stationary as implementations of the passive fathometer have used integration times[15] on the order of 100 s and the change in path length from a distant ship would be negligible over this time (moving sources are considered in Appendix B). Although only a single interferer is considered, here the results are easily generalized to multiple interfering sources as the contributions from multiple interferers add linearly provided the discrete sources are uncorrelated. A 16-element

array with equispaced elements of 0.18 m separation (design frequency, $f_d = 4167$ Hz and total length 2.88 m) in uniform sound speed of 1500 m/s was used. A similarly spaced array with 32 elements was used in Ref. 15. Here the number of array elements has been halved for clarity. The vertical noise was assumed to reflect off two layers at distances 50 and 58 m from the array bottom with reflection coefficients of 0.1 and 0.06, respectively.

The waveform used for both the vertical and interfering signals was a 60 μs box-car function which, when autocorrelated, becomes a triangle of width 120 μs. As the signal waveform is a narrow peak, the power spectrum of the signals is nearly flat. The vertical signal power spectrum was -20 dB relative to the power of the white noise. The discrete signal was assumed to be incident on the array via three multipaths with arrival angles of 5°, $-10°$, and 20° to broadside, with power spectra of 20, 0, and -20 dB, respectively, relative to the white noise. The path length differences of the three multipaths were 0, 20, and 45 m.

A sampling rate of $8f_d$ (33 kHz) was used to generate the signals and all processing was done with 2^{13} point Fourier transforms. The data for each signal were processed with two bandwidths, f_d (10−4167 Hz) which ensured no aliasing (see Sec. III B 1) occurred, and $4f_d$ (10−16.5 kHz). The large bandwidth allows the individual peaks described in Sec. II to be obtained. When computing the passive fathometer response with the large bandwidth, the response of each component of the CSDM (i.e., the CSDM formed from each possible combination of non-independent signals) was computed separately to prevent artifacts due to aliasing. The responses computed with a bandwidth of f_d were normalized with respect to the reflection peak at 50 m, and those computed with $4f_d$ were scaled to have the same peak magnitude as their small bandwidth counterparts.

The passive fathometer response computed with a bandwidth of f_d is shown in Fig. 4. Both the conventional and MVDR responses are dominated by peaks in the sensor noise region and both responses show peaks at ± 20 m from discrete noise. The seabed reflection peaks in the conventional response are not visible on this scale. The individual contributions from the fathometer model components are shown in Figs. 5–7.

1. Conventional response

The conventional passive fathometer response to each combination of signals is shown in Figs. 5 and 6. The cross-term between the up- and downward propagating signals gives δ-functions at the location of the reflecting layers at 50 and 58 m [Fig. 5(a)], consistent with T_1 of Eq. (15). The m^2 array gain increases the height of these peaks.

The component due to downward propagating noise gives a set of $m = 16$ equispaced peaks in the sensor noise region consistent with T_2 of Eq. (15) which contains a summation of m δ-functions spaced by τ. The right-most peak is a triangle with the left edge located at 0, consistent with a δ-function at 0 twice convolved with a box-car function. The width of the triangle is 120 μs $\times$ 1500 m/s $= 0.09$ m. These peaks grow broader when smaller bandwidths are processed.

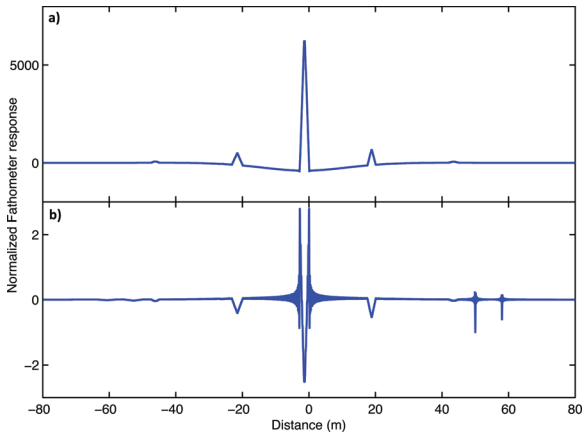

FIG. 4. (Color online) The conventional (a) and MVDR (b) passive fathometer response for the noise model described in Sec. III A computed with bandwidth of f_d (10–4167 Hz). The horizontal axis is the vertical distance corresponding to a two-way travel time. Both responses are normalized to the correlation peak due to the seabed reflection at 50 m.

When a bandwidth of f_d is used, the individual peaks merge into a single broad peak that spans the sensor noise region. The upward propagating noise gives multiple sets of δ-functions [Fig. 5(c)] consistent with T_3 of Eq. (15). In this case, η is a set of three δ-functions at -8, 0, and 8 m with heights of $[\Gamma_1\ \ \Gamma_2,\ \ \Gamma_1{}^2+\Gamma_2{}^2,\ \ \Gamma_2,\ \ \Gamma_1] = [0.006,\ \ 0.0136,\ \ 0.006]$. Note the upward propagating signal peaks are two orders of magnitude smaller than the downward [Figs. 5(b) and 5(c)], consistent with a reflection coefficient of 0.1. The term T_4 is not shown as it will neither interfere with the signal of interest (T_1) nor be the largest term in the noise correlation.

The white noise gives m equispaced peaks in the sensor noise region [Fig. 5(d), Eq. (7)], as do the autocorrelations of the three multipaths of the discrete signal [Figs. 6(a)–6(c), Eq. (20) with $\alpha = \beta$]. The response due to the three discrete

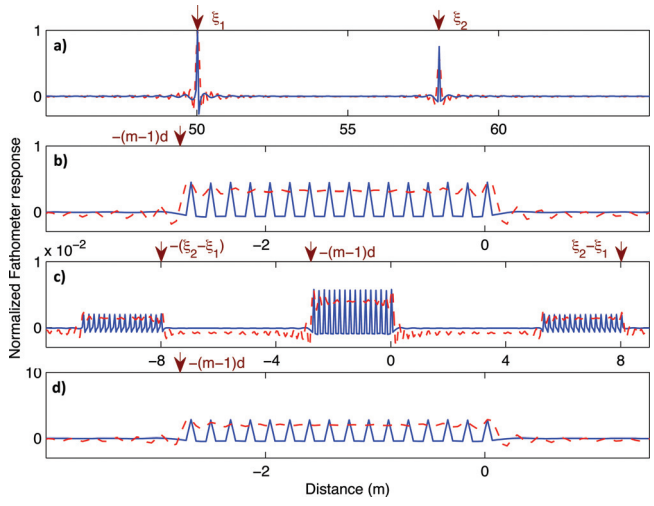

FIG. 5. (Color online) The conventional passive fathometer response computed with a bandwidth of $4f_d$(0–16.5 kHz, solid) and f_d(10–4167 Hz, dashed) to the following components of the CSDM plotted against the distance associated with a two-way travel time. (a) The cross-term between downward and upward propagating noise [T_1 from Eq. (15)], (b) downward propagating noise (T_2), (c) upward propagating noise (T_3), and (d) white noise.

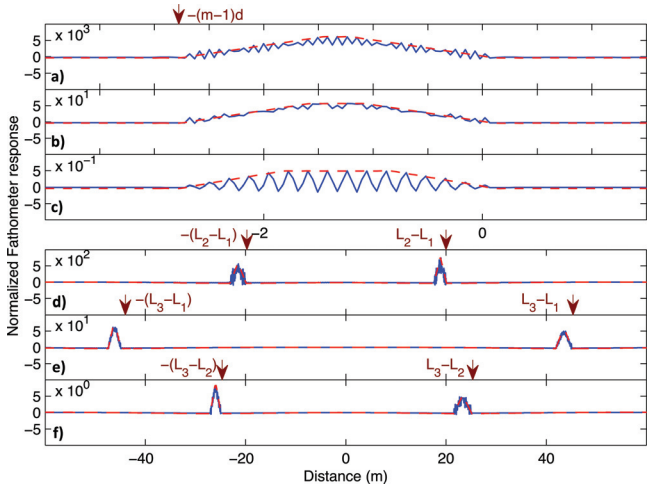

FIG. 6. (Color online) Same as Figs. 5(a)–5(c) the three multipath arrivals from the discrete source, (d)–(f) the cross-terms between the first and second, first and third, and second and third discrete source multipaths, respectively.

multipaths scale, as expected, with relative peak heights of 0, −20, and −40 dB.

The cross-terms associated with the discrete multipaths are the only terms producing a response in the positive time domain [Figs. 6(d)–6(f)] other than the seabed reflection (T_1). All three cross-terms give one set of peaks in the positive time domain and one set in the negative time domain. The right-most peak of both sets occurs at $\pm\omega/d$, which is consistent with Eq. (20) where ω is ±20, ±45, and ±25 m, respectively.

The smallest discrete cross-term [Fig. 6(f)] is larger than the vertical cross-term [Fig. 5(a)] and the other discrete cross-terms [Figs. 6(d) and 6(e)] are orders of magnitude larger still. Thus the dominant terms for $t > 0$ of the conventional passive fathometer response are due to the discrete source while the vertical seabed reflection is obscured, as shown in Fig. 4(a) in which the peak from Fig. 6(d) is the only prominent peak outside the sensor noise region.

2. MVDR response

In accordance with Eq. (24), the components of the conventional response were multiplied by $(-1/b_j + \sigma^2)$, except for the white noise term which was multiplied by σ^{-4}. In this case, σ was 1 and b_j is the trace of the CSDM associated with the jth coherent signal. The results are shown in Fig. 7.

All of the components have been multiplied by a negative factor, except the white noise, and the relative amplitudes are now different. The largest component is the white noise [Fig. 7(d)] followed by the vertical cross-term [Fig. 7(a)] which, in contrast to the conventional passive fathometer, is larger than the cross-term peaks due to the discrete source [Figs. 7(h)–7(j)].

Although the peaks have been rescaled relative to the conventional response, the locations have remained unchanged. This is consistent with Eq. (24) which shows that the CSDM inverse used in MVDR processing contains the same components as the CSDM rescaled by real multiplicative factors.

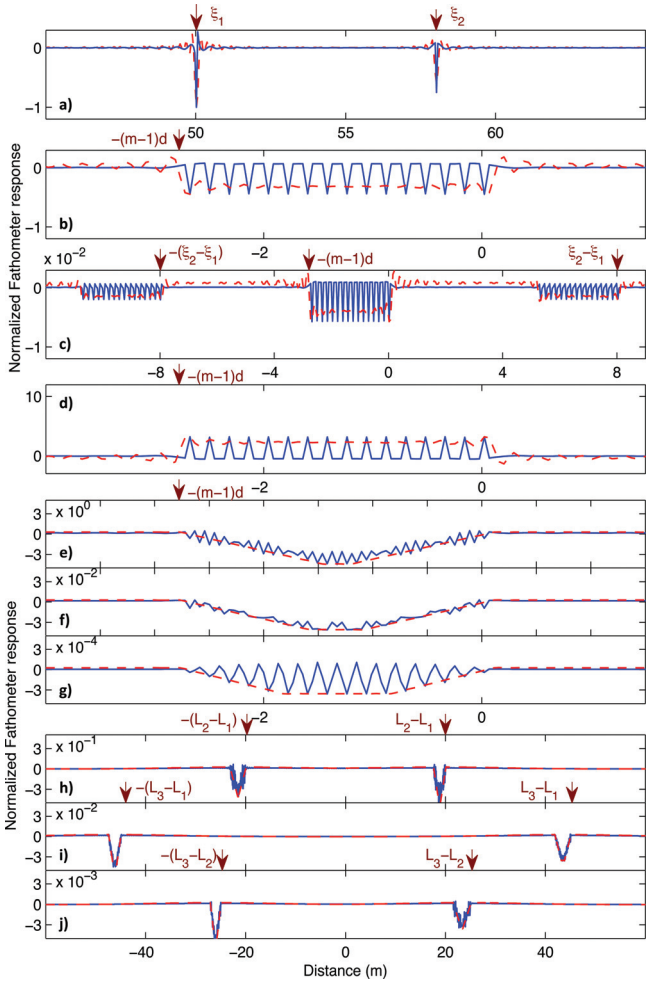

FIG. 7. (Color online) The MVDR passive fathometer response to the same components of the CSDM as shown in (a)–(d) Fig. 5 and (e)–(j) Fig. 6.

B. Three-dimensional surface noise model

The response of the passive fathometer to an infinite sheet of sources near the surface, as considered in Sec. II B 2, is now simulated. Only the surface noise is shown, as discrete interferers and sensor noise yield results very similar to those in Sec. III A. A wavenumber integration[29] simulation of the noise generated by an infinite two-dimensional ocean surface in a horizontally homogenous waveguide (based on the Kuperman–Ingenito noise model[18]) was constructed with a 32-element array of the same inter-element spacing as described in Sec. III A and sampling frequency 12 kHz. The array was situated with the lowest element at 70 m depth with reflecting layers at 120 m depth (the sediment layer) and at 122 m depth (the bottom). The sound speeds of the three layers were 1500, 1550, and 1580 m/s. The conventional and MVDR fathometer responses were computed using simulated CSDMs for all frequency bins from 10−4167 Hz of 4096-point Fourier transforms.

The results are shown in Fig. 8. The prominent features are the peaks in the sensor noise region [Figs. 8(a) and 8(c), equivalent to T_2 and T_3 from the 1D model, Eq. (13)], the reflection peaks at 50 and 52 m [Figs. 8(a) and 8(b), T_1 from Eq. (13)] and the reflection off the ocean surface at -70 ± 2 m [Figs. 8(a) and 8(d)]. This is consistent with two signals

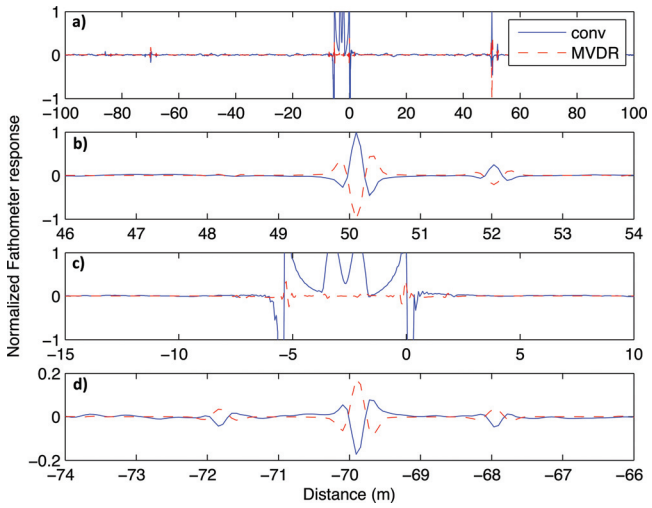

FIG. 8. (Color online) The wavenumber integration simulation of the conventional and MVDR passive fathometer response to an infinite sheet of noise at two-way travel time ranges of (a) −100 to 100, (b) 46–54, (c) −15 to 10, and (d) −74 to −66 m.

reflecting off the sediment with a relative time-delay corresponding to a 2 m propagation distance. Both reflect off the surface such that a correlation of the signals yields four correlation peaks with two at the same location. Hence the central peak is twice the height of the adjacent peaks as shown in Fig. 8(d). This term follows from Eq. (A10) in Appendix A, but not from Eq. (13) which did not include surface reflections. T_4, which is subject to less array gain than any of the other terms, is not visible in Fig. 8.

There is a close correspondence between the prominent features in this simulation (which includes signal from an infinite surface sheet) and Eq. (15) (which assumed only a small patch of surface directly above the array). This correspondence suggests, subject to appropriate array geometries and processing bandwidths, the approximation that vertically propagating noise is the dominant contribution is valid. While a detailed description of what geometries and bandwidths are required to validate this model is beyond the scope of this paper, the effect of bandwidth on the simulated response is considered in Sec. III B 1.

1. Exceeding the design frequency

The resolution that can be obtained by the fathometer is determined by the bandwidth used in the processing. However, as the array design frequency is exceeded, signals propagating in non-vertical directions alias into the beams steered to isolate vertically propagating noise. At frequency f any signal incident on the array at an angle,

$$\phi_\alpha = \pm \arcsin\left(1 + \frac{nc}{fd}\right), \tag{26}$$

will be added in phase and is thus subject to the same array gain as the vertically propagating noise. n is an integer value. As such, the fathometer response computed with frequencies above the design frequency will contain components from sound propagating in non-vertical directions. However, each frequency will contain energy aliased from a different angle of incidence. Integrating over a large bandwidth therefore results in the addition of many alias terms with different phases. These terms interfere and attenuate relative to the reflection peak, which is added in phase. Previous work has suggested that the ocean bottom reflection peak can be extracted when frequencies up to about twice the design frequency are used.[11]

To investigate the relationship between aliasing and the fathometer response, the simulated data were downsampled spatially to yield a sub-array containing every third element (10-elements with 0.54 m spacing and design frequency 1389 Hz). The fathometer response was constructed with a range of bandwidths with MVDR [Fig. 9(b)] passive fathometer processing. The minimum frequency used was 10 Hz and the upper frequency bound was varied from 100 to 6000 Hz.

The critical angle of the bottom θ_c is $\arccos(1500/1580) = 18.3°$. The surface sources produce sound propagating in all directions of which sound propagating at angles shallower than the critical angle experiences little attenuation. This implies that there is a discontinuity in the angular

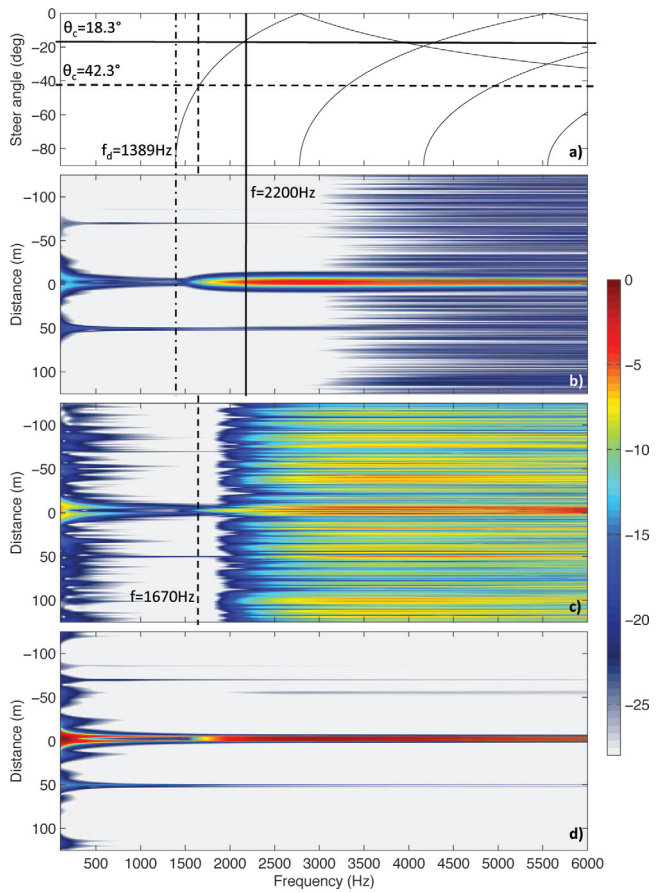

FIG. 9. (Color online) (a) Alias structure of the downsampled array ($f_d = 1389$ Hz). The critical angle of the simulated seabeds (horizontal lines), the design frequency (vertical dashed-dotted), and the frequencies at which significant signals alias into the vertical beams (vertical lines) are shown. The MVDR passive fathometer response computed with a lower frequency limit of 10 Hz and an upper limit shown on the horizontal axis is shown for (b) a bottom speed of 1580 m/s ($\theta_c = 18.3°$), (c) a bottom speed of 2030 m/s ($\theta_c = 42.3°$), and (d) a bottom speed of 1580 m/s and an array of vertical velocity sensors.

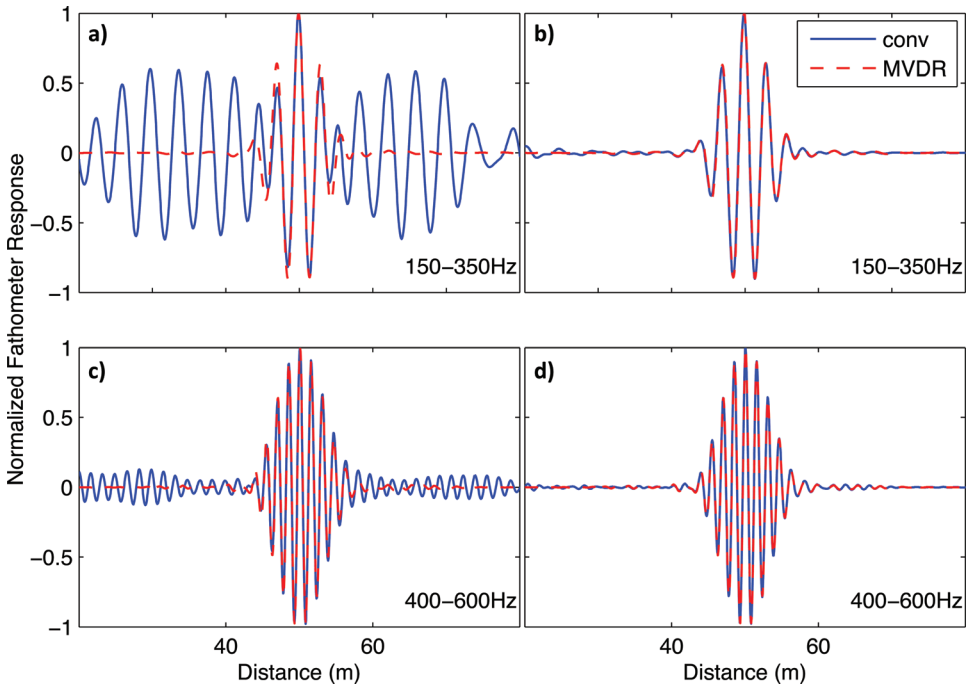

FIG. 10. (Color online) The simulated passive fathometer response for the full array ($f_d = 4167$ Hz) computed with a three layer simulation with sound speeds of 1500, 1550, and 1580 m/s and attenuations of (a and c) 0, 0.06, and 0.2 dB/λ and (b and d) 0, 1.06, and 1.2 dB/λ with (a and b) 150–350 and (c and d) 400–600 Hz. All plots were normalized with respect to the largest peak between 40 and 60 m. The MVDR trace has been multiplied by −1.

distribution of incident energy with more acoustic energy incident at angles shallower than θ_c than at steeper angles. As discussed in Appendix B, the stationary phase approximation is only valid for continuous noise distributions, and the presence of this discontinuity introduces spurious peaks in the passive fathometer response [Eq. (B6)]. These peaks are due to energy incident at θ_c and alias into the vertical beams at 2200 Hz [Fig. 9(a)]. When this frequency is included in the processing, the ocean bottom reflection peak is obscured [Fig. 9(b)]. Rearranging Eq. (26) gives this frequency as

$$f_{\max} = \frac{2fd}{(1+\sin\theta_c)}. \tag{27}$$

A harder seafloor will have a larger critical angle and is thus limited to a lower bandwidth, as shown in Fig. 9(c), which was computed with the same processing as the previous example but with a sediment sound speed of 2000 m/s and a seabed sound speed of 2030 m/s (critical angle of 42.3°). In this case, noise propagating at the critical angle aliases into the vertical beams at a frequency of 1670 Hz. At ~1800 Hz the reflection peak is obscured.

Use of vertical velocity sensors rather than pressure sensors makes the array more sensitive to vertically propagating energy, and previous work has shown that a single vertical velocity sensor can extract the bottom reflection from ambient noise.[11] Replacing the hydrophones in the low bottom-speed environment with vertical velocity sensors shows that the effect of the horizontal noise is significantly attenuated [Fig. 9(d)]. This extends the upper frequency boundary to beyond 6000 Hz (4.3 times the design frequency) allowing for a greater resolution. In this case the diagonal elements of the CSDM were set to zero to alter the dynamic range.

2. Error terms in the stationary phase approximation

The passive fathometer response in Eq. (18) is the leading order asymptotic behavior of an integration over an infinite surface source. Higher-order terms have been neglected thus far but they become significant at low frequencies and in the presence of spatial discontinuities in the noise field (see Appendix B). In order to produce significant error terms the discontinuity in the noise field must be sharp relative to the wavelength of the oscillatory term in the integral of Eq. (A5) and hence these error terms attenuate at high frequencies. The frequency dependence of these error terms is consistent with spurious peaks that appear in the passive fathometer response when only frequencies lower than 500 Hz are used [Figs. 9(c)–9(d); although not visible on this color-scale, they are also present in Fig. 9(b)].

The effect of these low frequency error terms is shown in Fig. 10. The conventional passive fathometer response is obscured when 150–350 Hz signals are processed [Fig. 10(a)]. Using the same model and bandwidth but higher frequencies (400–600 Hz) attenuates the spurious contributions [Fig. 10(b)]. Using the same frequency bands with increased seabed attenuation, which both decreases the horizontally propagating energy in the waveguide and softens the discontinuity in the noise field, attenuates the error terms [Figs. 10(c) and 10(d)]. MVDR processing is more robust to the influence of these error terms as they are produced, by definition, by non-vertical signals.

IV. CONCLUSION

An analytical fathometer model, verified by numerical simulation, has been presented that describes the asymptotic behavior of the passive fathometer to ambient noise components in a simple waveguide. The leading order term of the

surface noise yields the correlation of all possible vertical multipaths. The largest contribution is the correlation of the signal propagating directly from the surface with the signal reflecting from the seabed. This yields the travel time for sound to propagate from the array to seabed reflecting layers. Vertical noise correlations of other multipaths yield spurious peaks but they are localized and the largest are restricted to negative correlation times.

MVDR processing attenuates the contributions from non-vertical surface noise and discrete noise sources which may obscure the seabed reflection. Contributions from non-vertical surface noise become negligible at high frequencies (shown in Appendix B and Sec. III B 2) and in the presence of weakly reflective seabeds. Discrete noise incident on the array via multipaths generate localized peaks in the positive time domain of the passive fathometer response (Sec. II C).

The maximum frequency that can be used while avoiding the application of the array gain to non-vertical signals (i.e., spatial aliasing) is determined by the array geometry and seabed critical angle. In a shallow-water waveguide, there is a discontinuity in the spatial distribution of distant surface noise at the critical angle θ_c which produces error terms in the passive fathometer response. This becomes important when noise incident at θ_c aliases into the vertical beams. Thus the bandwidth available for passive fathometer processing may be increased to include frequencies above the design frequency f_d without inducing substantial errors, providing the maximum frequency processed does not exceed $2f_d/(1+\sin\theta_c)$.

ACKNOWLEDGMENTS

This work was supported by the Office of Naval Research, Grant Nos. N00014-05-1-0264 and N00014-08-1-0196.

APPENDIX A: ANALYTICAL MODEL OF PASSIVE FATHOMETER RESPONSE

Given the vector of data measured by the array, $\mathbf{d}(\omega)$, the CSDM is (see Sec. II)

$$\begin{aligned}\mathbf{R}(\omega) &= E[\mathbf{x}(\omega)\mathbf{x}^H(\omega)] \\ &= E\left[\int \mathbf{g}(\mathbf{r})s(r)2\pi r\,dr \int s(r')^*\mathbf{g}(r')^H 2\pi r'\,dr'\right] \\ &\quad + E\left[\sum_{j=1}^{J}\mathbf{g}_j n_j n_j^* \mathbf{g}_j^H\right] + E[\mathbf{u}\mathbf{u}^H] \\ &= |S(\omega)|^2 \int \mathbf{g}\mathbf{g}^H 2\pi r\,dr + \sum_{j=1}^{J}|N_j(\omega)|^2\mathbf{g}_j\mathbf{g}_j^H + \sigma^2\mathbf{I} \\ &= \mathbf{R}_c + \mathbf{R}_d + \mathbf{R}_w \qquad \text{(A1)}\end{aligned}$$

where we have defined the white noise component to be $E[\mathbf{u}\mathbf{u}^H] = \sigma^2\mathbf{I}$. The expectation of the correlation of the surface and discrete noise sources are defined to be $E[s(r)s(r')] = |S(\omega)|^2\delta(r-r')/(2\pi r)$ and $E[n_j n_j] = |N_j(\omega)|^2$, respectively. The Dirac-delta function, $\delta(r-r')/(2\pi r)$, results as the surface sources are assumed to be uncorrelated, consistent with previous surface noise models.[17] This allows the integral over r' to be eliminated which makes Eq. (1) tractable. $\mathbf{g}_j = \mathbf{g}(r_j, z_j)$ is the vector of Green's functions accounting for the possible multipaths from a source at $r = r_j$ and $z = z_j$ to each array element. Substituting this into Eq. (4) gives the fathometer response [Eq. (6)].

1. Discrete noise

Substituting the Green's function between a source at location $\mathbf{r}_j = (r_j, z_j)$ and a receiver at location $\mathbf{r}_p = (r_p, z_p)$ in a uniform waveguide with a single reflecting layer (i.e., the seabed) [Eq. (3) of Ref. 24 and Eq. (17) in the text] into the discrete term of Eq. (A1) gives the element of $\mathbf{R}_d$ in the pth row and qth column,

$$\begin{aligned}[\mathbf{R}_d]_{pq} &= \sum_{j=1}^{J}|N_j(\omega)|^2 g_p(r_j,z_j)g_q(r_j,z_j)^* \\ &= \sum_{j=1}^{J}|N_j(\omega)|^2 \sum_{\alpha,\beta}^{\infty}\frac{\Gamma^{b_\alpha+b_\beta}}{(4\pi)^2 L_\alpha L_\beta}e^{\imath(\omega/c)L_\Delta}, \qquad \text{(A2)}\end{aligned}$$

where $L_\Delta = L_\alpha - L_\beta$ and the path length $L_\alpha = \sqrt{r_j^2 + (2b_\alpha\Delta \pm z_p \pm z_j)^2}$. Applying the steering vectors, the contribution to the fathometer response from the discrete noise is given by

$$\begin{aligned}C_d(\omega) &= \mathbf{w}^T\mathbf{R}_d\mathbf{w} = \sum_{j=1}^{J}\sum_{p,q=1}^{m}\sum_{\alpha,\beta}^{\infty}|N_j(\omega)|^2 \\ &\quad \times \frac{\Gamma^{b_\alpha+b_\beta}}{(4\pi)^2 L_\alpha L_\beta}\psi^{(p+q-2)+(L_\Delta/d)}, \qquad \text{(A3)} \\ &= \sum_{j=1}^{J}\sum_{p,q=1}^{m}\sum_{\alpha,\beta}B(j,p,q,\alpha,\beta)\psi^{\mu(j,p,q,\alpha,\beta)}, \qquad \text{(A4)}\end{aligned}$$

which describes a set of delta functions in the time domain with amplitude $B = |N_j(\omega)|^2\frac{\Gamma^{b_\alpha+b_\beta}}{(4\pi)^2 L_\alpha L_\beta}$ at location $-\mu\tau = -(p+q-2)\tau - \frac{L_\Delta}{c}$.

2. Correlated noise

The analysis of the correlated noise component is similar to that of the discrete noise component, but the summation over sources is now replaced by an integral over an infinite sheet. Substituting Eq. (17) into the correlated term of Eq. (A1) gives the elements of the CSDM due to the correlated noise component as

$$[\mathbf{R}_c]_{pq} = \frac{|S(\omega)|^2}{(4\pi)^2}\sum_{\alpha,\beta}^{\infty}\Gamma^{b_\alpha+b_\beta}\int_{r=0}^{\infty}\frac{e^{\imath kL_\Delta}}{L_\alpha L_\beta}2\pi r\,dr, \qquad \text{(A5)}$$

where the path length is $L_\alpha = \sqrt{r^2 + (2b_\alpha\Delta \pm z_p)^2}$.

The integral in Eq. (A5) is evaluated by stationary phase approximation, in which the integral $\int e^{ikf(r)}2\pi r\,dr$ is assumed to be dominated by contributions near the stationary point of

$f(r)$.[30] This interference is more pronounced with a large value of k and thus this approximation becomes more accurate with increasing frequency. Using $f = L_\Delta$ gives

$$\frac{df}{dr} = r\left(\frac{1}{L_\alpha} - \frac{1}{L_\beta}\right), \frac{d^2f}{dr^2} = \frac{1}{L_\alpha} - \frac{1}{L_\beta} - \frac{r}{L_\alpha^3} + \frac{r}{L_\beta^3}. \quad \text{(A6)}$$

Equation (A6) shows that there is one stationary point at $r = 0$. Assuming $p \neq q$ and substituting the first two non-zero terms of the Taylor expansion of f around $r = 0$ in Eq. (A5) gives

$$[\mathbf{R}_c]_{pq} = \frac{|S(\omega)|^2}{(4\pi)^2} \sum_{\alpha,\beta} \Gamma^{b_\alpha + b_\beta} \frac{e^{\imath k(\tilde{z}_\alpha - \tilde{z}_\beta)}}{\tilde{z}_\alpha \tilde{z}_\beta} \int_{r=0}^{\infty} e^{\imath k(r^2/2)\Theta} 2\pi r\, dr, \quad \text{(A7)}$$

where the following substitutions have been made,

$$\begin{aligned} f(r=0) &= L_\alpha(r=0) - L_\beta(r=0) \\ &= (2b_\alpha\Delta \pm z_p) - (2b_\beta\Delta \pm z_p) = \tilde{z}_\alpha - \tilde{z}_\beta, \end{aligned} \quad \text{(A8)}$$

$$\left.\frac{d^2f}{dr^2}\right|_{r=0} = \frac{1}{\tilde{z}_\alpha} - \frac{1}{\tilde{z}_\beta} = \Theta. \quad \text{(A9)}$$

Making the substitution $u = r\, e^{\imath\pi/4}\sqrt{k\Theta/2}$ gives

$$[\mathbf{R}_c]_{pq} = \frac{-\imath|S(\omega)|^2}{8\pi k} \sum_{\alpha,\beta} \Gamma^{b_\alpha + b_\beta} \frac{e^{\imath k(\tilde{z}_\alpha - \tilde{z}_\beta)}}{\tilde{z}_\alpha - \tilde{z}_\beta}. \quad \text{(A10)}$$

For simplicity, we assume no surface bounce occurs (α can take one of the two values: $\alpha = 0$ denotes the direct path from surface to the pth element and $\alpha = 1$ denotes a single bottom bounce) which implies

$$\begin{aligned} \tilde{z}_0 - \tilde{z}_0 &= z_q - z_p = (q-p)d \\ \tilde{z}_0 - \tilde{z}_1 &= z_p - (2\Delta - z_q) = -(\tilde{z}_1 - \tilde{z}_0) \\ \tilde{z}_1 - \tilde{z}_1 &= (2\Delta - z_p) - (2\Delta - z_q) = (q-p)d, \end{aligned} \quad \text{(A11)}$$

where the constraint of no surface bounce reduces the $\pm z_p$ term in $\tilde{z}_\alpha$ to $-z_p$.

Substituting $z_p = z_\alpha - (p-1)d$ and $\xi_0 = 2(\Delta - z_\alpha)$, Eq. (A10) then becomes

$$\begin{aligned} [\mathbf{R}_c]_{pq} = \frac{-\imath c|S(\omega)|^2}{8\pi\omega} \Bigg[& (1+\Gamma^2)\frac{\psi^{(q-1)}}{(q-p)d} \\ & + \Gamma \frac{\psi^{-(p+q-2)\xi_0/d} + \psi^{(p+q-2)+\xi_0/d}}{\xi_0 + (p+q-2)d} \Bigg] \forall p \neq q. \end{aligned} \quad \text{(A12)}$$

Applying the steering vectors gives Eq. (18).

APPENDIX B: ERROR TERMS IN THE STATIONARY PHASE APPROXIMATION

1. Frequency-dependent error terms

We are concerned with integrals of the general form

$$I = \int_{r=a}^{b} F(r) e^{\imath k f(r)} dr = \int_{r=a}^{b} \frac{F}{\imath k \frac{df}{dr}} \frac{d}{dr}(e^{\imath k f}) dr, \quad \text{(B1)}$$

$$= \left.\frac{F}{\imath k \frac{df}{dr}} e^{\imath k f}\right|_{r=a}^{b} - \frac{1}{\imath k}\int_{r=a}^{b} \frac{d}{dr}\left(\frac{F}{\frac{df}{dr}}\right) e^{\imath k f} dr, \quad \text{(B2)}$$

where we have integrated by parts. Note that the same integration by parts can be repeated *ad infinitum*, as the integral in Eq. (B2) is of the same form as that in Eq. (B1). This yields an infinite series expansion of I. Each successive integration brings another factor of $1/(\imath k)$ and thus at high frequencies the behavior of I is dominated by the first term.

It is the behavior of the leading order term of I, with limits $a = 0$ and $b = \infty$, that was derived in Appendix A and yields the depth of the seabed reflecting layers. Contributions from higher-order terms in the expansion, although not evaluated explicitly here, become increasingly significant at low frequencies. These terms may be the cause of the spurious peaks in the fathometer response at low frequencies as shown by simulation in Sec. III B 2.

2. Effect of seabed critical angle

In the previous use of the stationary phase approximations the seabed reflection coefficient, Γ was assumed independent of grazing angle. This is clearly not the case, as for rays incident on the seabed at angles shallower than the critical angle, the reflection coefficient is one. Here we consider a fathometer model where the reflection coefficient varies as a step function such that

$$\Gamma_\alpha(r) = \begin{cases} \gamma & \theta \leq \theta_c \\ 1 & \theta \geq \theta_c, \end{cases} \quad \text{(B3)}$$

where $\gamma < 1$ is a constant. As the stationary phase approximation used in Appendix A is only valid for continuous functions, Eq. (A12) is not correct for this case. Defining $\epsilon_\alpha = (2b_\alpha\,\Delta \pm z_\alpha)/\tan\theta_c$ as the radial distance from the array at which rays from the α path are incident upon the ocean bottom at the critical angle θ_c and experience no attenuation from bottom loss, Eq. (A5) becomes

$$\begin{aligned} [\mathbf{R_c}]_{pq} = \frac{|S(\omega)|^2}{(4\pi)^2} \sum_{\alpha,\beta} \Bigg[& \gamma^{b_\alpha + b_\beta} \int_{r=0}^{\epsilon_\alpha} \frac{e^{\imath k(L_\alpha - L_\beta)}}{L_\alpha L_\beta} 2\pi r\, dr \\ & + \gamma^{b_\beta} \int_{r=\epsilon_\alpha}^{\epsilon_\beta} \frac{e^{\imath k(L_\alpha - L_\beta)}}{L_\alpha L_\beta} 2\pi r\, dr + \int_{r=\epsilon\beta}^{\infty} \frac{e^{\imath k(L_\alpha - L_\beta)}}{L_\alpha L_\beta} 2\pi r\, dr \Bigg], \end{aligned} \quad \text{(B4)}$$

where $\epsilon_\beta > \epsilon_\alpha$.

The first term can be evaluated as in Appendix A and yields the same result [Eq. (A10)]. The other two terms cannot be evaluated by the stationary phase approximation as they have no stationary points within the limits of integration [conversely, the first term cannot be evaluated by the following method as the stationary point produces an infinite term when the limit $r = 0$ is substituted into Eq. (B2)].

Substituting $F = 2\pi r/(L_\alpha L_\beta)$ and $f = L_\Delta$ and into the leading order term of Eq. (B2) yields

$$I \approx \frac{2\pi}{\imath k(L_\beta - L_\alpha)} e^{\imath k L_\Delta}\Big|_{r=a}^{b} = \frac{2\pi}{\imath k}\left[\frac{e^{\imath k L_\Delta(a)}}{L_\Delta(a)} - \frac{e^{\imath k L_\Delta(b)}}{L_\Delta(b)}\right]. \quad \text{(B5)}$$

Substituting this into Eq. (B4) with the appropriate limits of integration yields

$$[\mathbf{R}_c]_{pq} = \frac{-\imath|S(\omega)|^2}{8\pi k}\sum_{\alpha,\beta}\left[\gamma^{b_\alpha+b_\beta}\frac{e^{\imath k(\tilde{z}_\alpha-\tilde{z}_\beta)}}{\tilde{z}_\alpha-\tilde{z}_\beta} + \gamma^{b_\beta}\frac{e^{\imath kL_\Delta(\alpha)}}{L_\Delta(\alpha)} + (1-\gamma^{b_\beta})\frac{e^{\imath kL_\Delta(\beta)}}{L_\Delta(\beta)}\right|. \quad \text{(B6)}$$

The second and third terms are error terms introduced by discontinuities in the noise field at the critical angle. Such discontinuities might be expected in a waveguide with low attenuation in the seabed and low scattering. If $\Gamma_\alpha(r)$ is not infinitely discontinuous, at high enough frequencies the wavelength of the oscillatory function $e^{\imath k(L_\alpha-L_\beta)}$ at $r=\epsilon$ is small enough that $\Gamma_\alpha(r)$ appears continuous and these error terms attenuate. Thus these error terms attenuate at high frequencies. As these terms are due to energy incident at the critical angle, their contribution to the passive fathometer response may be attenuated by the use of MVDR steering vectors which more effectively excludes non-vertical noise.

Increased attenuation in the seabed will reduce the discontinuity in the spatial distribution of incident noise and may decrease the effect of these terms.

3. Moving sources

Data must be averaged over a finite amount of time in order to approximate the CSDM [Eq. (5)]. A discrete source that moves from $\mathbf{r}_1$ to $\mathbf{r}_2$ during this integration time will produce a similar effect on the CSDM [Eq. (A2)] as a spatially distributed source that varies continuously between $\mathbf{r}_1$ and $\mathbf{r}_2$ and is zero elsewhere,

$$[\mathbf{R}_d]_{pq} = \frac{|N(\omega)|^2}{|\mathbf{r}_1-\mathbf{r}_0|}\sum_{\alpha,\beta}^{\infty}\frac{\Gamma^{b_\alpha+b_\beta}}{(4\pi)^2}\int_{\mathbf{r}_0}^{\mathbf{r}_1}\frac{e^{\imath(\omega/c)L_\Delta}}{L_\alpha L_\beta}d\mathbf{r}. \quad \text{(B7)}$$

For any given combination of paths α and β this gives an integral of the form in Eq. (B5), which yields

$$[\mathbf{R}_d]_{pq} = \frac{-\imath|N(\omega)|^2}{8\pi k|\mathbf{r}_1-\mathbf{r}_0|}\sum_{\alpha,\beta}^{\infty}\Gamma^{b_\alpha+b_\beta}\left(\frac{e^{\imath(\omega/c)L_\Delta(\mathbf{r}_0)}}{L_{\Delta(\mathbf{r}_0)}}+\frac{e^{\imath(\omega/c)L_\Delta(\mathbf{r}_1)}}{L_{\Delta(\mathbf{r}_1)}}\right). \quad \text{(B8)}$$

This is similar to the contribution produced by stationary sources [Eq. (A2)] but is scaled by the $1/(k|\mathbf{r}_1-\mathbf{r}_0|)$ and thus the maximum contribution would be expected from stationary sources.

[1] J. Rickett and J. Claerbout, "Acoustic daylight imaging via spectral factorization: He-lioseismology and reservoir monitoring," The Leading Edge **18**, 957–960 (1999).
[2] R. L. Weaver and O. I. Lobkis, "Ultrasonics without a source: Thermal fluctuation correlations at MHz frequencies," Phys. Rev. Lett. **87**, 134301 (2001).
[3] P. Roux and W. A. Kuperman, "Extracting coherent wave fronts from acoustic ambient noise in the ocean," J. Acoust. Soc. Am. **116**, 1995–2005 (2004).
[4] P. Roux, K. G. Sabra, W. A. Kuperman, and A. Roux, "Ambient noise cross-correlation in free space: Theoretical approach," J. Acoust. Soc. Am. **117**, 79–84 (2005).
[5] O. A. Godin, "Recovering the acoustic Green's function from ambient noise cross-correlation in an inhomogeneous moving medium," Phys. Rev. Lett. **97**, 053401 (2006).
[6] L. A. Brooks and P. Gerstoft, "Green's function approximation from cross-correlations of 20-100Hz noise during a tropical storm," J. Acoust. Soc. Am. **125**, 723–734 (2009).
[7] M. J. Buckingham and S. A. S. Jones, "A new shallow-ocean technique for determining the critical angle of the seabed from the vertical directionality of the ambient noise in the water column," J. Acoust. Soc. Am. **81**, 938–946 (1987).
[8] N. M. Carbone, G. B. Deane, and M. J. Buckingham, "Estimating the compressional and shear wave speeds of a shallow water seabed from the vertical coherence of ambient noise in the water column," J. Acoust. Soc. Am. **103**, 801–813 (1998).
[9] C. H. Harrison and D. G. Simons, "Geoacoustic inversion of ambient noise: A simple method," J. Acoust. Soc. Am. **112**, 1377–1389 (2002).
[10] M. Siderius, C. H. Harrison, and M. B. Porter, "A passive fathometer technique for imaging seabed layering using ambient noise," J. Acoust. Soc. Am. **120**, 1315–1323 (2006).
[11] P. Gerstoft, W. S. Hodgkiss, M. Siderius, C. F. Huang, and C. H. Harrison, "Passive fathometer processing," J. Acoust. Soc. Am. **123**, 1297–1305 (2008).
[12] C. H. Harrison and M. Siderius, "Bottom profiling by correlating beam-steered noise sequences," J. Acoust. Soc. Am. **123**, 1282–1296 (2008).
[13] C. H. Harrison, "Anomalous signed passive fathometer impulse response when using adaptive beam forming," J. Acoust. Soc. Am. **125**, 3511–3513 (2009).
[14] J. Traer, P. Gerstoft, H. C. Song, and W. S. Hodgkiss, "On the sign of the adaptive passive fathometer impulse response," J. Acoust. Soc. Am. **126**, 1657–1658 (2009).
[15] M. Siderius, H. C. Song, P. Gerstoft, W. S. Hodgkiss, and C. H. Harrison, "Adaptive passive fathometer processing," J. Acoust. Soc. Am. **127**, 2193–2200 (2010).
[16] S. L. Means and M. Siderius, "Effects of sea-surface conditions on passive fathometry and bottom characterization," J. Acoust. Soc. Am. **126**, 2234–2241 (2009).
[17] B. F. Cron and C. H. Sherman, "Spatial correlation functions for various noise models," J. Acoust. Soc. Am. **34**, 1732–1236 (1962).
[18] W. A. Kuperman and F. Ingenito, "Spatial correlation of surface generated noise in a stratified ocean," J. Acoust. Soc. Am. **67**, 1988–1996 (1980).
[19] C. H. Harrison, "Formulas for ambient noise level and coherence," J. Acoust. Soc. Am. **99**, 2055–2066 (1996).
[20] C. H. Harrison, "Performance and limitations of spectral factorization for ambient noise sub-bottom profiling," J. Acoust. Soc. Am. **118**, 2913–2923 (2005).
[21] A. B. Baggeroer, W. A. Kuperman, and H. Schmidt, "Matched field processing: Source localization in correlated noise as an optimum parameter estimation problem," J. Acoust. Soc. Am. **83**, 571–587 (1988).
[22] H. Nakahara, "A systematic study of theoretical relations between spatial correlation and Green's function in one-, two- and three-dimensional random scalar wavefields," Geophys. J. Int. **167**, 1097–1105 (2006).
[23] R. Snieder, K. Wapenaar, and K. Larner, "Spurious multiples in seismic interferometry of primaries," Geophysics **71**, Sl111–Sl124 (2006).
[24] L. A. Brooks and P. Gerstoft, "Ocean acoustic interferometry," J. Acoust. Soc. Am. **121**, 3377–3385 (2007).
[25] H. L. van Trees, *Optimum Array Processing* (Wiley, New York, 2002), Chap. 2.
[26] F. B. Jensen, W. A. Kuperman, M. B. Porter, and H. Schmidt, *Computational Ocean Acoustics* (Springer-Verlag, New York, 2000), Chap. 2.
[27] K. G. Sabra, P. Roux, and W. A. Kuperman, "Arrival-time structure of the time-averaged ambient noise cross-correlation function in an oceanic waveguide," J. Acoust. Soc. Am. **117**, 164–174 (2005).
[28] H. L. van Trees, *Optimum Array Processing* (Wiley, New York, 2002), Chap. 6.
[29] H. Schmidt, *OASES Version 3.1 User Guide and Reference Manual* (MIT, Cambridge, 2004).
[30] C. M. Bender and S. A. Orszag, *Advanced Mathematical Methods for Scientists and Engineers: Asymptotic Methods and Perturbation Theory* (McGraw-Hill, New York, 1978), Chap. 6.